Research Article

Zhengdong Deng, Zhao Lu*, Guangyuan Wang*, Daqing Wang, Zhibin Ding, Hongfei Zhao, Haoli Xu, Yue Shi, Zijian Cheng, and Xiaoning Zhao

Extraction of fractional vegetation cover in arid desert area based on Chinese GF-6 satellite

https://doi.org/10.1515/geo-2020-0241
received January 10, 2021; accepted March 10, 2021

Abstract: The red edge band is considered as one of the diagnosable characteristics of green plants, but the large-scale remote sensing retrieval of fractional vegetation coverage (FVC) based on the red edge band is still rare. To explore the application of the red edge band in the remote sensing estimation of FVC, this study proposed a new vegetation index (normalized difference red edge index, RENDVI) based on the two red edge bands of Chinese GaoFen-6 satellite (GF-6). The FVC estimated by using three vegetation indices (NDVI, $RENDVI_1$, and $RENDVI_2$) were evaluated based on the field survey FVC obtained in Minqin Basin of Gansu Province. The results showed that there was a good linear correlation between the FVC estimated by GF-6 WFV data and the FVC investigated in the field, and the most reasonable estimation of FVC was obtained based on $RENDVI_2$ model ($R^2 = 0.97611$ and RMSE = 0.07075). Meanwhile, the impact of three confidence levels (1, 2, and 5%) on FVC was also analyzed in this study. FVC obtained from NDVI and $RENDVI_2$ has the highest accuracy at 2% confidence, while FVC based on $RENDVI_1$ achieved the best accuracy at 5% confidence. It could be concluded that it is feasible and reliable to estimate FVC based on red edge bands, and the GF-6 Wide Field View (WFV) data with high temporal and spatial resolution provide a new data source for remote sensing estimation of FVC.

Keywords: vegetation index, pixel dichotomy model, fractional vegetation cover, red edge band

1 Introduction

As an important part of the ecosystem, the changes of vegetation in its quantity and population proportion will lead to changes in land surface energy, biogeochemical cycle, and hydrology, which is one of the most important links in global change [1–3]. To measure the surface vegetation coverage and its changes effectively and quantitatively, the researchers used the concept of fractional vegetation coverage (FVC) [4,5]. FVC is defined as the percentage of the vertical projection area of vegetation (including branches, stems, and leaves) on the ground to the total area of the statistical area [6]. As a comprehensive quantitative index reflecting the surface conditions of vegetation community coverage, FVC is widely used in the ecological environment assessment [7], groundwater enrichment assessment [8], groundwater level monitoring [9], soil degradation, and desertification monitoring [10].

The traditional surface measurement methods for FVC include the photographic method, the sample strip method, the sample point method, the spatial quantitative meter, and so on [11]. Although the accuracy of FVC obtained by these methods is high, due to the characteristics such as small measurement range, time consumption, laborious, and easy to be restricted by natural conditions, these methods cannot measure the FVC of large areas, and the application value is very limited. With the development of remote sensing technology, remote sensing monitoring based on the relationship between vegetation spectral information and vegetation coverage has become the main technical means to obtain FVC in large areas [12]. The current data sources for remote sensing estimation of FVC mainly include Landsat, MODIS (Moderate-resolution Imaging Spectroradiometer), GaoFen (GF), SPOT (Systeme Probatoire d'Observation de la Terre), and so on

* **Corresponding author: Zhao Lu,** Defense Engineering College, Army Engineering University, Nanjing 210007, China, e-mail: zhaoxiacyj@126.com
* **Corresponding author: Guangyuan Wang,** Defense Engineering College, Army Engineering University, Nanjing 210007, China
Zhengdong Deng, Daqing Wang, Zhibin Ding, Haoli Xu, Yue Shi, Zijian Cheng, Xiaoning Zhao: Defense Engineering College, Army Engineering University, Nanjing 210007, China
Hongfei Zhao: Postdoctoral workstation of Jinling Hospital, Nanjing 210016, China

[13–16]. The commonly used bands are mainly the blue band (450–520 nm), the green band (520–590 nm), the red band (630–690 nm), and the near infrared band (770–890 nm). The vegetation indices proposed based on the bands include the normalized green-red difference index (NGRDI) [17], the normalized green-blue difference index (NGBDI) [18], the visible-band difference vegetation index (VDVI) [19], and the normalized difference vegetation index (NDVI) [20]. Although the research methods based on these vegetation indices showed good accuracy in many remote sensing estimations of FCV, there were not many applications of FVC estimation in arid and semi-arid regions [21]. Due to the sparse vegetation distribution and special vegetation types in arid and semi-arid areas, a few scholars thought that those general model methods may lose their universal applicability [22].

The red edge band (670–760 nm) is between the red band and the near infrared band. Currently, the researches of remote sensing based on the red edge band mainly includes land classification, chlorophyll content, and biomass at three levels: ground hyperspectral, aviation hyperspectral, and satellite image [23–26]. Some studies showed that the red edge band can effectively reflect the specific spectral characteristics of crops, and thus, it was considered as one of the diagnosable characteristics of green plants [27,28]. However, the application of the red edge band to the remote sensing estimation of FVC in arid and semi-arid regions is still very rare.

Previously, the main satellite images for the red edge band application study were Rapid Eye [29], EO-1 (Earth Observing-1) Hyperion [30], and Sentinel-2 [31]. Due to the lack of available sensors, the effect of the red edge band on FVC estimation has not attracted much attention [32]. Fortunately, in addition to the common visible and near infrared bands, Chinese GaoFen-6 (GF-6) satellite WFV (Wide Field View) ta also covers two red edge band bands, which provides a new data source for large-scale estimation of vegetation coverage, and there is no research on FVC inversion based on GF-6 data before.

The purpose of this study is to construct a new vegetation index based on the characteristics of GF-6 satellite WFV data and to put forward a new reliable remote sensing estimation method for FVC in an arid environment. Taking sparse vegetation in the arid desert area as the research objective, this article discusses the application of the red edge band in remote sensing estimation of FVC by comparing with the field survey data.

2 Data

2.1 Study area

The study area (38°19′47″–38°44′50″N, 102°48′15″–103°19′1″E) is located on Minqin County, Wuwei City, Gansu Province, China, with an area of about 2,100 km^2 (Figure 1). It is adjacent to the Tengger Desert in the east and the Badain Jaran Desert in the west, which have a typical arid desert climate. The geomorphic types are mainly mountains, plains, and sand dunes, with an altitude of 1,400–2,100 m. The natural vegetation in the study includes *Nitraria sphaerocarpa*, *Salsola passerina*, *Reaumuria soongarica*, *Ephedra przewalskii*, *Alhagi sparsifolia*, and *Rtemisia desertorum*, while the artificial vegetation mainly includes *Haloxylon ammodendron*, *Elaeagnus angustifolia*, and *Hedysarum scoparium* [33].

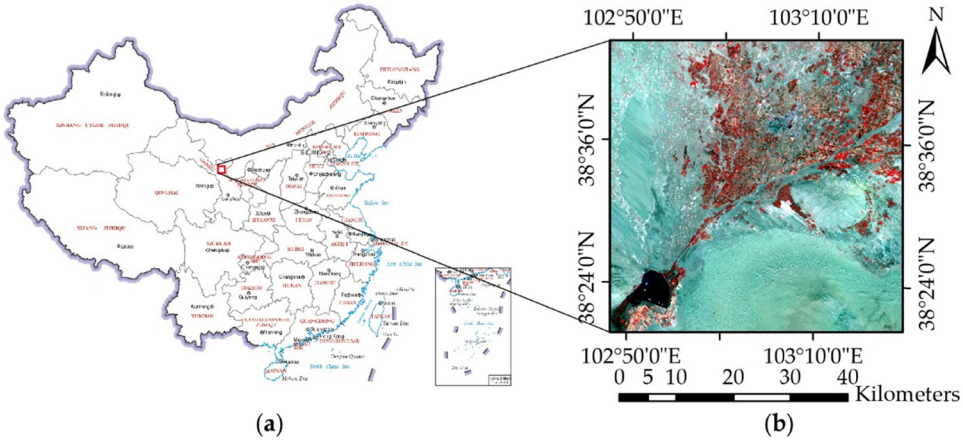

Figure 1: The location of the study area. (a) The red rectangle is the geographic location of the study area. (b) The true color image of GaoFen-6 satellite (GF-6) image after preprocessing.

2.2 GF-6 WFV data

The Chinese GaoFen-6 satellite (GF-6) was officially put into use on March 21, 2019. It is a low-orbit optical remote sensing satellite, using the CAST 2000 platform. The satellite is equipped with a 2 m panchromatic/8 m multispectral high-resolution camera (PMS) and a 16 m multispectral medium-resolution WFV camera. The observation width of PMS is 90 km and that of WFV is 800 km. The time resolution is 4 days. The GF-6 WFV sensor covers 8 bands. Compared with the GF-1 satellite, in addition to the common four bands (blue, green, red, and near infrared), it also adds two red edge bands, purple band and yellow band. The technical specification for GF-6 WFV data is presented in Table 1.

The GF-6 WFV data used in this study were obtained from the Land Survey Satellite Data Service Platform of the China Resources Satellite Application Center. The satellite image was acquired on September 29, 2019, and the weather in the study area was sunny and cloudless. Affected by the adverse factors such as atmosphere, light, and terrain, a remote sensing image may be distorted due to geometric deformation, noise interference, and other reasons; therefore, it is necessary to preprocess the data to get the real surface reflectance. In this study, ENVI 5.5 software was used to complete the radiometric calibration, atmospheric correction, geometric correction, image cropping, and other preprocessing work for the acquired satellite images. Figure 1b shows the true color image of the GF-6 satellite image after preprocessing.

2.3 Field survey FVC

To evaluate the accuracy of FVC estimated by remote sensing, a field survey of FVC was also conducted in the study area. According to the geomorphology and the vegetation coverage type of the study area, 16 sampling points were set up in the study area, and the latitude and longitude coordinates were obtained by UniStrong GPS instrument. The selection of the sampling points followed the rules that the vegetation types and coverage within 2×2 pixels (32 m × 32 m) were basically the same. Ten samples were randomly selected at each sampling point, and the size of each sample was 2 m × 2 m. Nikon D7100 digital camera was used to take a photo of the sample at a height of 2 m above the ground. For the convenience of taking pictures, the 2 m × 2 m sample square was divided into four 1 m × 1 m sample squares. After the photo was taken, the four 1 m × 1 m small sample photos were corrected, spliced, and interpreted indoors to obtain the vegetation coverage of the 2 m × 2 m sample. Photoshop software was used to interpret the spliced images. By adjusting hue, saturation and brightness, and other steps, the interpreted images with a gray value were obtained. Through visual interpretation, pixels with a gray value greater than 125 were identified as vegetation pixels, and the proportion of these pixels in the image was calculated, so that the measured vegetation coverage could be obtained.

Figure 2 shows the actual photographs and the interpreted renderings of wheat and *Haloxylon ammodendron*. In the interpreted image, the bright pixels are vegetation, and the dark pixels are other features. Then, the measured FVC of the sample can be obtained by counting the percentage of bright pixels in the entire image. The average FVC of all samples was taken as the FVC of the sampling point.

3 Methodology

3.1 Estimation model of FVC

The remote sensing estimation methods of FVC mainly include the regression model method, the machine

Table 1: Technical specification of GaoFen-6 Wide Field View (GF-6 WFV) data used in this study

Band number	Channel	The range of spectrum (nm)	The temporal resolution (d)	The spatial resolution (m)
1	Blue	450–520	4	16
2	Green	520–590		
3	Red	630–690		
4	Near infrared	770–890		
5	Red edge 1	690–730		
6	Red edge 2	730–770		
7	Purple	400–450		
8	Yellow	590–630		

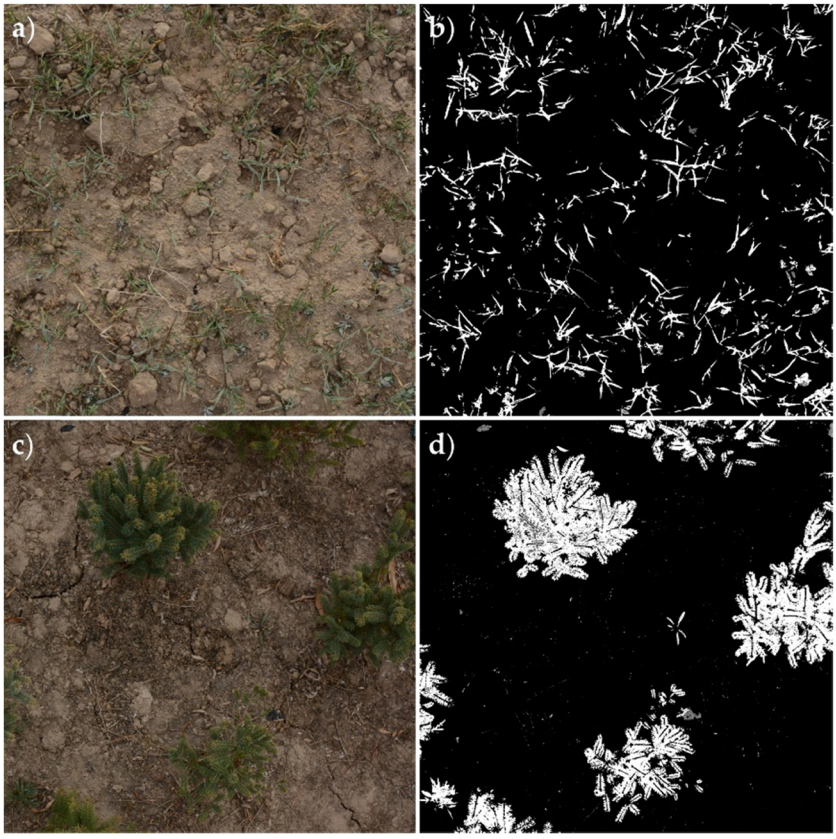

Figure 2: Interpretation of the measured fractional vegetation cover. Images of (a) wheat and (c) *Haloxylon ammodendron* taken on-site. Interpretation results of (b) wheat and (d) *H. ammodendron*.

learning method, the mixed pixel decomposition model method, and so on. The regression model method estimates FVC by establishing linear or nonlinear regression relationships between certain bands or vegetation indices of remote sensing data and measured FVC. The commonly used bands in the regression model method include the red band, the green band, and the near infrared band [34]. The vegetation indices that have been studied are normalized differential vegetation index (NDVI) [35], enhanced vegetation index (EVI) [36], and modified vegetation index (MVI) [37]. The regression model method is simple and easy to implement, and the estimation accuracy of FVC on a small scale is also high. However, this method is not suitable for large-scale and low-resolution remote sensing data because of the high requirements on the number of measured data.

The common machine learning methods include the neural network [38], decision tree [39], support vector machine [40], and so on. According to the different training samples, machine learning methods can be divided into two categories: one based on remote sensing image classification [41] and the other based on a radiation transfer model [42,43]. Although the accuracy of FVC estimated by the machine learning method is high, the complex surface, sample selection, and model training will all affect the overall accuracy. In areas where there are scarce samples available for model training, the applicability of machine learning methods is limited.

The mixed pixel decomposition model assumes that each component in the pixel contributes to the observation of the remote sensing sensor, and the FVC is estimated by decomposing this mixed pixel. Mixed pixel decomposition models can be divided into linear and nonlinear models. The pixel dichotomy model is a kind of linear mixed pixel model and was also widely used with good effect [44–46]. The advantage of this model is that it still can be used without the measured FVC data. Based on the actual conditions of the study, the pixel dichotomy model method was chosen as the estimation model of FVC.

The assumption of the pixel dichotomy model is that the images captured by satellites only contain vegetation and soil. That is, at a certain pixel, there is a single vegetation, a single soil, or both ground objects. At this time,

buildings, rivers, and other ground objects are not considered in the model. The pixel dichotomy model assumes that pixels in remote sensing satellite images consist of only vegetation and soil. In other words, the information S captured by the remote sensor can be linearly synthesized by S_V contributed by the vegetation and S_S contributed by the soil [47]:

$$S = S_V + S_S. \tag{1}$$

Assuming that the proportion of vegetation coverage in a pixel is f_c, it can be considered that FVC in that pixel is f_c, and then, the proportion of bare soil is $1 - f_c$. Assuming that the remote sensing information obtained by pure pixels covered by all vegetation is S_{Veg}, then the spectral response contributed by vegetation in the mixed pixels can be expressed as the product of S_{Veg} and f_c:

$$S_V = f_c \times S_{Veg}. \tag{2}$$

Similarly, assuming the remote sensing information obtained by pure pixels all covered by soil is S_{Soil}, and the information S_S contributed by soil in the mixed pixel can be expressed as the product of S_{Soil} and $1 - f_c$:

$$S_S = (1 - f_c) \times S_{Soil}. \tag{3}$$

Based on equations (1)–(3), the spectral response of a mixed pixel can be derived:

$$S = S_V + S_S = f_c \times S_{Veg} + (1 - f_c) \times S_{Soil}. \tag{4}$$

Then, the FVC can be obtained by modifying equation (4) as follows:

$$f_c = (S - S_{Soil})/(S_{Veg} - S_{Soil}). \tag{5}$$

3.2 Vegetation index

The pixel dichotomy model requires that the remote sensing information used must have a good linear relationship with the FVC. Therefore, it is necessary to select the appropriate remote sensing information for the mixed pixel, photosynthetic vegetation end element, and soil end element. It is very limited to extract vegetation information by analyzing and comparing individual or multiple single-band data, but the vegetation index can better reflect the vegetation information. To this end, the reflection characteristics of ground objects in different bands need to be studied.

According to the actual investigation results, four types of features including plant, water body, desert, and bare soil were selected, and the reflectance of the pixels completely covered by these features was extracted from the preprocessed GF-6 image. The reflection characteristics of these typical features in different bands are shown in Figure 3.

Figure 3 shows that, except water body, the reflectance of the other three types of ground objects in the near infrared (B4), red edge 1 (B5), and red edge 2 (B6) bands is higher than that in the other bands. In particular, the reflectance of plant pixels in the near infrared band and the red edge 2 band is much higher than that in the red edge 1 band. According to the spectral characteristics exhibited by plant in the red edge bands, this study attempted to construct a new vegetation index based on red edge bands to invert FVC.

Among the many vegetation indices, NDVI is believed to partially eliminate the effects of changes in radiometric conditions related to the solar altitude angle, satellite observation angle, terrain, clouds, shadows, and atmospheric conditions. NDVI was also a commonly used parameter source in the estimation of vegetation coverage by the pixel dichotomy model [48–50]. In this study, NDVI was used to compare with the remote sensing estimation of FVC based on the new vegetation index. NVDI is calculated as follows:

$$\mathrm{NDVI} = \frac{\mathrm{NIR} - \mathrm{RED}}{\mathrm{NIR} + \mathrm{RED}}. \tag{6}$$

In equation (6), NIR and RED are the reflectance of pixels in the near infrared band and the red band, respectively.

With reference to the definition of NDVI, a new vegetation index based on the red edge band is proposed: normalized difference red edge index (RENDVI). RENDVI is calculate as follows:

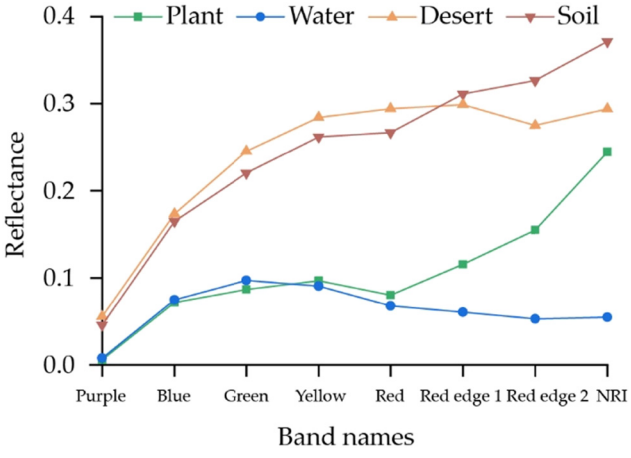

Figure 3: Reflectance of typical features in different bands.

$$\mathrm{RENDVI} = \frac{\mathrm{RE} - \mathrm{RED}}{\mathrm{RE} + \mathrm{RED}}. \quad (7)$$

In equation (7), RE is the reflectance of pixels in the red edge band, and RED is the reflectance of pixels in the red band. Since there are two red edge bands in the WFV data, the normalized difference red edge index based on the red edge 1 band and the red edge 2 band is recorded as RENDVI_1 and RENDVI_2, respectively.

3.3 Remote sensing estimating of FVC

Two parameters S_{Soil} and S_{Veg} in equation (5) were required to estimate FVC when using the pixel dichotomy model. These two parameters are usually determined by the measured method and the confidence method. In this study, the confidence method was used to extract S_{Soil} and S_{Veg} from the vegetation index due to the large area of research and the small number of measured samples. The researchers used different confidence levels in their respective FVC studies [51–53]. To compare the influence of confidence on the estimation results, according to the gray distribution of the vegetation index extracted from the entire image, the upper and lower thresholds of the vegetation index were intercepted with confidence levels of 1, 2, and 5%. That is, the vegetation index values with cumulative frequencies of 1, 2, and 5%, respectively, were recorded as S_{Soil}, and the vegetation index values with cumulative frequencies of 99, 98, and 95, respectively, were recorded as S_{Veg}. Then, the FVC thematic map based on a certain vegetation index under different confidence levels can be produced.

3.4 Accuracy evaluation

In this study, the field measured FVC and the FVC estimated based on the pixel dichotomy model were regressed and fitted. The accuracy of the FVC estimated by remote sensing was evaluated by calculating the determination coefficient (R^2) and root-mean-square error (RMSE). For the fitting result, if the R^2 is high and the RMSE is low, it means that the accuracy of remote sensing estimation is high. RMSE measured the overall estimation accuracy and could not check the estimation accuracy of each sample point. Therefore, the relative measurement error (RME) was also calculated to check the estimation accuracy of each sample point. Equations (8), (9) and (10) are the calculation methods of R^2, RMSE and RME, respectively.

$$R^2 = \sum_{i=1}^{n} (\widehat{P_i} - \overline{P})^2 \Big/ \sum_{i=1}^{n} (P_i - \overline{P})^2, \quad (8)$$

$$\mathrm{RMSE} = \sqrt{\sum_{i=1}^{n} (\widehat{P_i} - \overline{P})^2 \Big/ n}, \quad (9)$$

$$\mathrm{RME} = (\widehat{P_i} - P_i)/P_i. \quad (10)$$

In equations (8)–(10), $\widehat{P_i}$ represents the estimated value of FVC remote sensing of the ith sample point; P_i represents the field survey FVC of the ith sample point; $\bar{P}$ represents the average FVC of the measured sample points; and n is the number of sample points.

4 Results

4.1 Field survey FVC of sample points

The FVC interpretation results of the sample points in the study area are presented in Table 2. The 16 sites covered four types of vegetation: *H. ammodendron*, wheat, low bush, and white poplar. The vegetation at sample point 13 was a cluster of woods near Hongyashan Reservoir where the foliage was very lush, and the measured FVC was also the largest, reaching 0.9967. Sample point 11 was located on the edge of the Tengger Desert, with scarce vegetation and the smallest FVC, i.e., only 0.0122.

4.2 Vegetation indices extraction results

Based on equations (6) and (7), ENVI 5.5 software was used to obtain NDVI, RENDVI_1 and RENDVI_2, and the

Table 2: Field survey of fractional vegetation coverage (FVC) of sample points

Sample number	FVC	Sample number	FVC
1	0.2722	9	0.0311
2	0.2756	10	0.0456
3	0.2011	11	0.0122
4	0.2322	12	0.9956
5	0.1267	13	0.9967
6	0.2867	14	0.5011
7	0.4089	15	0.2989
8	0.2333	16	0.2322

results are shown in Figure 4. The statistical results of the three vegetation indices are presented in Table 3.

Table 3: Statistical results of the three vegetation indices

Vegetation index	Min value	Max value	Average value	Standard deviation
NDVI	−0.340858	0.760981	0.0849	0.1122
$RENDVI_1$	−0.174256	0.350569	0.0309	0.03504
$RENDVI_2$	−0.370259	0.733248	0.05029	0.0991

4.3 FVC estimation based on different vegetation indices

According to the extraction results of vegetation indices, the values of S_{Soil} and S_{Veg} under different confidence levels are presented in Table 4.

Substituting the S_{Soil} and S_{Veg} values from Table 4 into equation (5), the FVC can be obtained based on three vegetation indices under different confidence levels. According to the corresponding relationship between soil erosion intensity surface erosion classification and FVC in China's 'Classification Standards for Soil Erosion Classification, the FVC in the study area was divided into five levels: the lowest coverage (0–0.3), the lower coverage (0.3–0.45), the medium coverage (0.45–0.6), the higher coverage (0.6–0.75), and the highest coverage (0.75–1). The normal FVC should be between 0 and 1, but the FVC of some ground features (such as water bodies and shadows) may be less than 0. Therefore, it is necessary to remove the outliers from the calculation results. The usual operation method is to assign these pixels to 0.

According to the classification standards, the FVC estimation results in the study area are shown in Figures 5–7. Under the different confidence conditions, the estimation results based on different vegetation indices are significantly different. Figure 5 shows significantly more areas with lower coverage than Figures 6 and 7, which was particularly evident in Figure 5b. The areas covered by different levels of vegetation coverage shown in Figures 6 and 7 are similar, but Figure 7 shows significantly more pixels with vegetation coverage of 0 than Figures 5 and 6.

Tables 5–7 present pixel statistics of FVC grading results estimated by different vegetation indices at 1, 2, and 5% confidence level, respectively. The statistical results presented in Tables 5–7 show the vegetation coverage under different grades more accurately. The statistical results of pixels were consistent with the description of the inversion chart mentioned earlier. Under the 1% confidence level, the proportion of pixels contained in each grade was obviously different based on the inversion results obtained by the three indices, especially the difference between low vegetation coverage and low vegetation coverage was the most obvious. Under the two confidence levels of 2 and 5%, the number of pixels contained in each level in the inversion results obtained by different vegetation indices was different, but the proportion was similar. The proportion of pixels contained in the higher coverage level was very similar in all the inversion results.

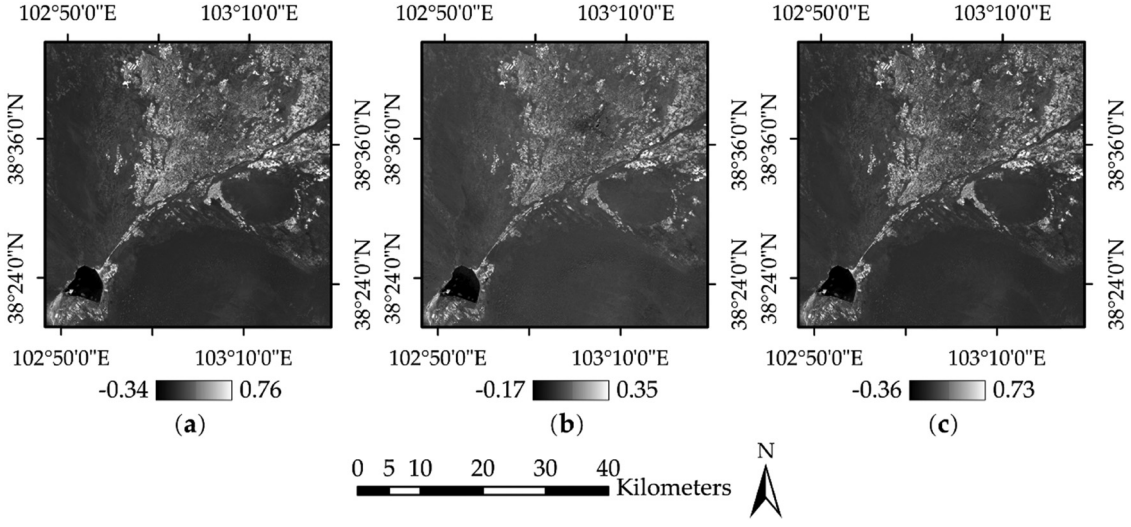

Figure 4: Extraction results of (a) normalized differential vegetation index (NDVI), (b) normalized difference red edge index 1 ($RENDVI_1$), and (c) normalized difference red edge index 2 ($RENDVI_2$).

Table 4: The values of S_{Soil} and S_{Veg} under different confidence levels

Vegetation index	1%		2%		5%	
	S_{Soil}	S_{Veg}	S_{Soil}	S_{Veg}	S_{Soil}	S_{Veg}
NDVI	−0.088083	0.482281	−0.016788	0.426108	−0.008164	0.331047
$RENDVI_1$	−0.039448	0.158133	−0.005489	0.135494	0.000685	0.100505
$RENDVI_2$	−0.108627	0.418941	−0.037273	0.358148	−0.028624	0.263279

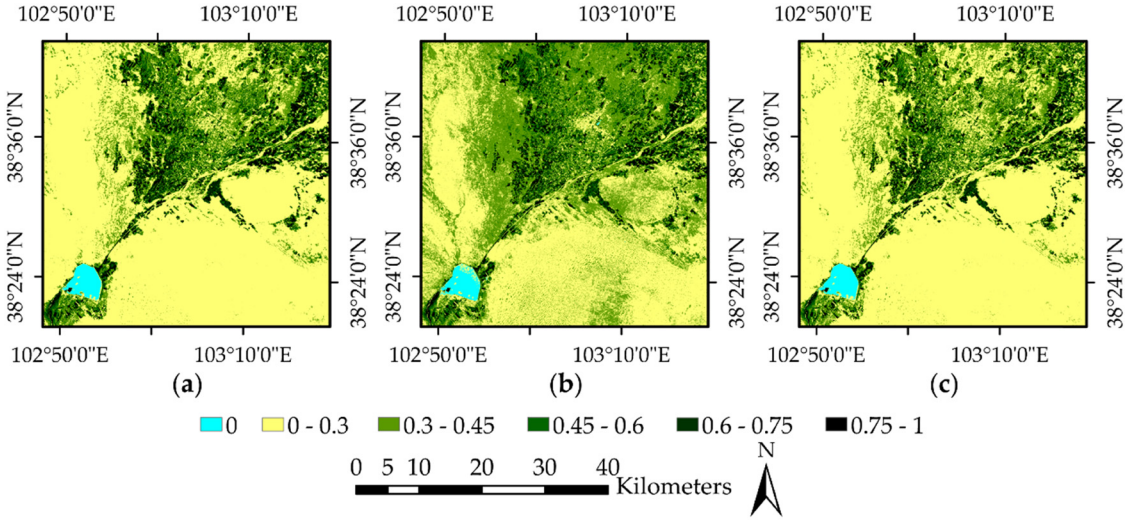

Figure 5: FVC estimation results based on (a) NDVI, (b) $RENDVI_1$, and (c) $RENDVI_2$ under 1% confidence.

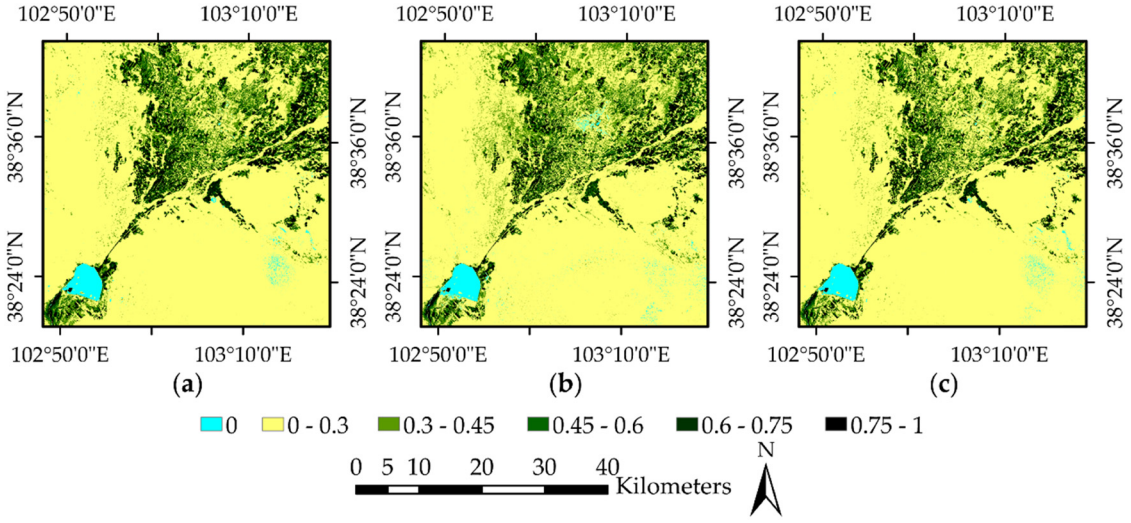

Figure 6: FVC estimation results based on (a) NDVI, (b) $RENDVI_1$, and (c) $RENDVI_2$ under 2% confidence.

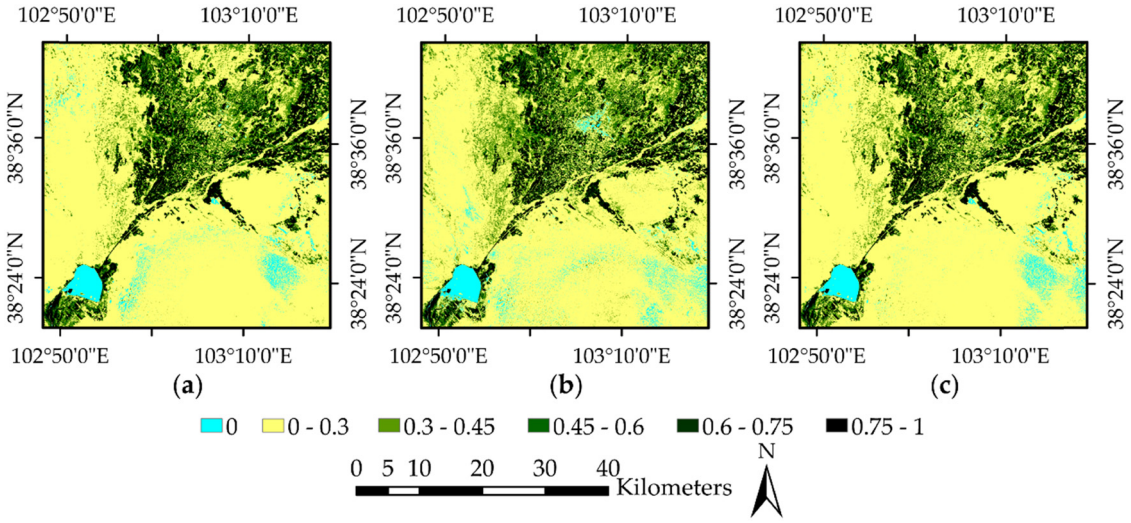

Figure 7: FVC estimation results based on (a) NDVI, (b) $RENDVI_1$, and (c) $RENDVI_2$ under 5% confidence.

4.4 Fitting results of correlation between measured FVC and estimated FVC by remote sensing

To assess the accuracy of remote sensing estimation FVC, the linear regression model between the field measured FVC and the FVC estimated by remote sensing is established. R^2 and RMSE were calculated according to equations (8) and (9), and the results are shown in Figure 8.

4.5 Error analysis of remote sensing estimation of FVC in sample points

To investigate the estimation accuracy of FVC of each sample point in the study area, the RME was calculated according to equation (10), and the results are shown in Figures 9–11.

Figure 11 shows that the RME of most sample points is small. However, when the confidence is 1%, the RME of sample points 9, 10, and 11 is high, especially sample point 11. The results show that when the confidence is 1%, the estimation accuracy of FVC in the desert edge with sparse vegetation is relatively poor.

5 Discussion

5.1 Analysis of different vegetation indices extraction results

Table 3 presents statistics on the extraction results of three vegetation indices in the study area. It can be seen from the table that the values of NDVI, $RENDVI_1$, and $RENDVI_2$ are −0.340858 to 0.760981, −0.174256 to 0.350569, and −0.370259 to 0.733248, respectively. In general, the value range of NDVI and $RENDVI_2$ is close, while that of $RENDVI_1$ is relatively narrow. As shown in Figure 3, the reflectance of ground objects in the red edge 1 band is lower than that in the near infrared band and the red edge 2 band, and hence, the value range of $RENDVI_1$ is different from that of NDVI and $RENDVI_2$.

Table 5: Pixel statistics of FVC grading results estimated by different vegetation indices at 1% confidence

Grading standards	NDVI	%	$RENDVI_1$	%	$RENDVI_2$	%
0	80,664	1.0	78,979	1.0	80,602	1.0
0–0.3	5,286,970	65.3	3,668,751	45.3	5,388,301	66.5
0.3–0.45	1,431,207	17.7	2,963,075	36.6	1,494,900	18.5
0.45–0.6	582,358	7.2	709,201	8.8	503,129	6.2
0.6–0.75	329,782	4.1	332,161	4.1	287,842	3.6
0.75–1	388,671	4.8	347,485	4.3	344,878	4.3

Table 6: Pixel statistics of FVC grading results estimated by different vegetation indices at 2% confidence

Grading standards	NDVI	%	$RENDVI_1$	%	$RENDVI_2$	%
0	111,026	1.4	133,255	1.6	116,312	1.4
0–0.3	5,983,771	73.9	5,877,837	72.6	6,176,159	76.3
0.3–0.45	831,920	10.3	978,067	12.1	775,250	9.6
0.45–0.6	429,001	5.3	430,850	5.3	362,254	4.5
0.6–0.75	275,149	3.4	256,180	3.2	236,897	2.9
0.75–1	468,785	5.8	423,463	5.2	432,780	5.3

5.2 Analysis of FVC remote sensing estimation results

Figure 8 shows that, in general, R^2 values of the fitting results based on the three vegetation indices are all above 0.9, which indirectly indicates that it is feasible and reliable to use the pixel dichotomy model to estimate FVC. By comparing and analyzing the estimation results based on the three vegetation indices, under the same confidence level, the fitting degree of vegetation coverage estimated based on $RENDVI_2$ is always the highest. Under the 2% confidence, the R^2 of FVC based on $RENDVI_2$ is 0.97635, which is the best of all results. These comparative analysis results show that the vegetation index based on the red edge bands proposed can be effectively used for FVC estimation.

5.3 Influence of confidence levels on FVC remote sensing estimation

In this study, to explore the influence of confidence on FVC estimation, the results of remote sensing estimation of FVC under three different confidence levels were compared. For NDVI and $RENDVI_2$, when the confidence level is 2%, the R^2 values of the estimation results are the largest, which are 0.97115 and 0.97635, respectively; for $RENDVI_1$, when the confidence level is 5%, the R^2 of the estimation result is the largest, which is 0.95981. When the confidence level is 1%, the R^2 values of the estimation results based on the three vegetation indices are the smallest, which are 0.96559, 0.96726, and 0.94723, respectively. For a certain vegetation index, when confidence is used to determine S_{Soil} and S_{Veg}, it does not mean that the greater the confidence, the better the FVC estimation results, or the lower the confidence, the better the FVC estimation results. The results of this article show that it is feasible to use the confidence method to extract S_{Soil} and S_{Veg} when FVC is estimated by the pixel bisection model, even if there is no large amount of the measured data. However, the impact of different confidence levels on the estimated results is clearly visible. Therefore, to obtain better accuracy, it is necessary to select the appropriate confidence level according to the specific conditions of the study area.

5.4 Vegetation coverage of study area

Figures 5–7 and Tables 5–7 show that the pixels with minimum vegetation coverage (0–0.3) and low vegetation coverage (0.3–0.45) account for a large proportion in the study area. In addition, except for Hongyashan Reservoir and other water bodies, the proportion of pixels with FVC of 0 is not large, indicating that there are few areas without vegetation coverage. Although the study area is surrounded by the Tengger Desert and the Badain Jaran Desert, the local government and residents have

Table 7: Pixel statistics of FVC grading results estimated by different vegetation indices at 5% confidence

Grading standards	NDVI	%	$RENDVI_1$	%	$RENDVI_2$	%
0	241,532	3.0	303,426	3.7	240,653	3.0
0–0.3	5,388,864	66.5	5,142,104	63.5	5,507,465	68.0
0.3–0.45	897,246	11.1	1,097,779	13.6	912,142	11.3
0.45–0.6	502,344	6.2	514,405	6.4	453,322	5.6
0.6–0.75	312,281	3.9	305,558	3.8	269,158	3.31
0.75–1	757,385	9.4	736,380	9.1	716,912	8.9

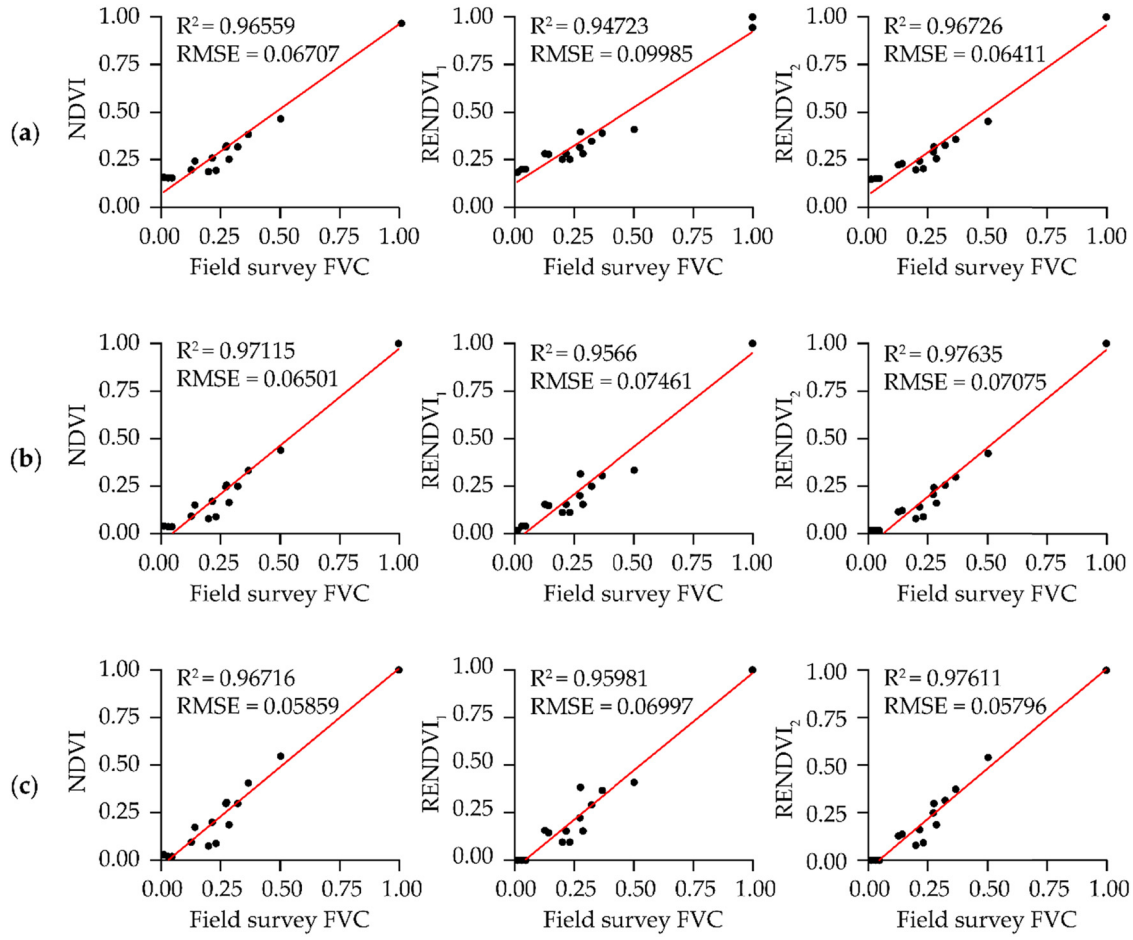

Figure 8: Linear fitting results between the field survey FVC and the FVC estimated by remote sensing under three confidence levels of (a) 1%, (b) 2%, and (c) 5%.

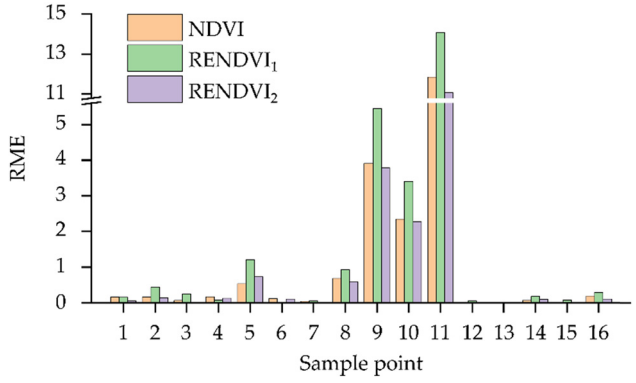

Figure 9: RME of sample points under 1% confidence.

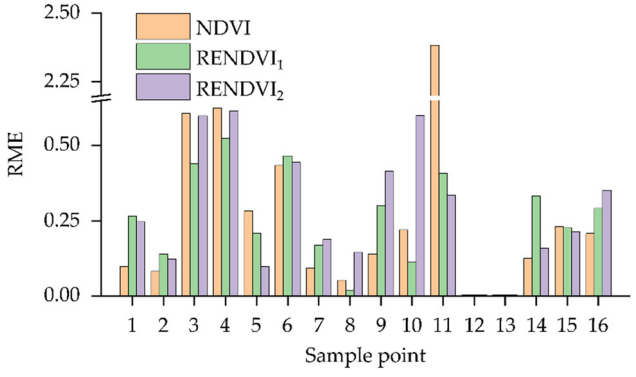

Figure 10: RME of sample points under 2% confidence.

taken measures in recent years to strictly control groundwater exploitation and actively transform the desert. *H. ammodendron* and other vegetation have gradually appeared in many areas completely covered by desert, which effectively improved the local desertification status [54].

It is worth noting that when the confidence is 1%, in the estimation results of FVC based on $RENDVI_1$, the proportion of pixels with FVC of 0–0.3 is significantly lower than that of other cases under the condition of 1% confidence, while the proportion of pixels with FVC of 0.3–0.45 is significantly higher than that of other eight

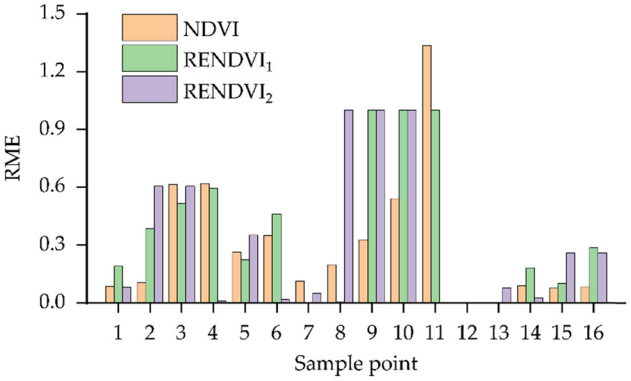

Figure 11: RME of sample points under 5% confidence.

cases. The possible reason for this phenomenon is that the range of $RENDVI_1$ is narrow. After extracting the relevant parameters of the pixel dichotomy model with 1% confidence, the model would enlarge the FVC of some sparse vegetation coverage areas.

5.5 Analysis of estimation error and uncertainty

The error sources of this study mainly include the selection of sample points for verification, the field survey FVC of sample points, and remote sensing images.

First, it is well known that it is impossible to completely match the position of the measured points on the ground with the corresponding points on the remote sensing image when there is no obvious reference feature. Therefore, it was required that the vegetation difference near the sample points used for verification should not be too large. In the selection of sample points, the principle of little difference in vegetation type and coverage within the range of 2×2 pixels ($32\,m \times 32\,m$) was followed as far as possible, and the field investigation of FVC would not be affected by the vegetation type and the coverage around the sample points consequently.

Second, due to the limitation of test conditions, the field survey FVC was estimated by photographing. Ten samples were randomly selected in each sample point, and the average FVC of all samples was regarded as the FVC of the sample point. The size of each sample is only $2\,m \times 2\,m$, while that of the sample point is $32\,m \times 32\,m$. The randomness of sample selection will affect the calculation of FVC to a certain extent. However, the size of the sample point is larger than that of the pixel, and the vegetation difference within a sample point is small; therefore, the error caused by sample selection can be ignored.

Finally, in the process of imaging, there will be deformation and dislocation for various reasons in remote sensing images, but these phenomena will be corrected to a large extent after radiation calibration, atmospheric correction, and geometric correction.

6 Conclusion

In this study, GF-6 WFV data were used as the data source, and the FVC estimation results based on NDVI, $RENDVI_1$, and $RENDVI_2$ were compared to explore the application of the red edge band in remote sensing estimation of FVC. Some useful conclusions are obtained.

The vegetation indices ($RENDVI_1$ and $RENDVI_2$) based on the red edge bands proposed in this paper showed good results in the remote sensing estimation of FVC. Whether using NDVI, $RENDVI_1$, or $RENDVI_2$, the estimated FVC based on the GF-6 WFV data had a good linear correlation with the field measured FVC. In terms of accuracy, the accuracy of FVC based on $RENDVI_1$ was worse than that based on $RENDVI_2$ and NDVI. The accuracy of FVC estimated based on $RENDVI_2$ and NDVI was close, but the overall accuracy of $RENDVI_2$ was better. At the 2% confidence, the model based on $RENDVI_2$ generated the best reasonable FVC estimation ($R^2 = 0.97611$ and RMSE = 0.07075). Studies had shown that the red edge band has a greater advantage in FVC remote sensing estimation in a large-scale background. The vegetation indices defined by the red edge bands of GF-6 WFV data and the FVC estimation method used in this paper can provide a meaningful reference for FVC remote sensing estimation.

According to the principle of the pixel dichotomy model, in theory, S_{Soil} should be close to 0 and S_{Veg} should be close to 1. However, due to various factors such as atmospheric conditions, regions, and vegetation types, these two parameters often change. In this study, three confidence levels (1, 2, and 5%) were used to determine S_{Soil} and S_{Veg} of the model and FVC, respectively. In general, the choice of confidence had an obvious influence on the estimation result of FVC, but there was no general law. At 2% confidence, FVC obtained from NDVI and $RENDVI_2$ has the highest accuracy, while FVC based on $RENDVI_1$ achieved the best accuracy at 5% confidence. When using the pixel dichotomy model to estimate FVC, a reasonable confidence level should be selected based on the land cover and satellite image characteristics of the study area.

In this study, due to various reasons such as equipment and personnel, the photographic method was used to measure the actual vegetation coverage. Due to the limited sample area observed by the camera method, the number and accuracy of the measured samples bring certain difficulties and influences to the verification of FVC. The arid area of Minqin, Gansu Province, was only taken as the research object. The remote sensing estimation method of FVC proposed in the study still needs to be widely verified in different climate and environment areas. At the same time, in order to improve the reliability of verification, it is very important to further enrich the measured FVC date. If conditions permit in the future, high-resolution UAV platform or other more advanced methods can be used to measure FVC, which may be more conducive to the verification of remote sensing estimation of FVC, thereby further promoting the development of this study.

Acknowledgments: The authors would deeply appreciate the anonymous reviewers and the editor for their constructive comments and suggestions, all of which have led to great improvements in the presentation of this article.

Author contributions: Z. D. and Z. L.: conceptualization; Z. L.: methodology; Z. L and G. W.: software; D. W. and Z. D.: validation; H. Z.: formal analysis; G. W. and H. X.: investigation; H. Z. and X. Z.: data curation; Z. L. and G. W.: writing – original draft preparation; Y. S. and Z. C.: writing – review and editing; Z. D.: project administration. All authors have read and agreed to the published version of the manuscript.

Funding information: This research received no external funding.

Conflict of interest: The authors declare no conflict of interest.

References

[1] Parmesan C, Yohe G. A globally coherent fingerprint of climate change impacts across natural systems. Nature. 2003;421(6918):37–42. doi: 10.1038/nature01286.

[2] Mu XH, Song WJ, Gao Z, McVicar TR, Donhue RJ, Yan GJ. Fractional vegetation cover estimation by using multi-angle vegetation index. Remote Sens Environ. 2018;216:44–56. doi: 10.1016/j.rse.2018.06.022.

[3] Yao YJ, Liang SL, Cheng J, Lin Y, Jia K, Liu M. Impacts of deforestation and climate variability on terrestrial evapotranspiration in subarctic China. Forests. 2014;5(10):2542–60. doi: 10.3390/f5102542.

[4] Gitelson AA, Kaufman YJ, Stark R, Rundquist D. Novel algorithms for remote estimation of vegetation fraction. Remote Sens Environ. 2002;80(1):76–87. doi: 10.1016/S0034-4257(01)00289-9.

[5] Jiapaer G, Chen X, Bao AM. A comparison of methods for estimating fractional vegetation cover in arid regions. Agric For Meteorol. 2011;151(12):1698–710. doi: 10.1016/j.agrformet.2011.07.004.

[6] Zhang WB, Fu SH, Liu BY. Error assessment of visual estimation plant coverage. J Beijing Norm Univ (Nat Sci). 2001;37(3):402–8. doi: 10.3321/j.issn:0476-0301.2001.03.026.

[7] Feng L, Hu WY, Li YX, Zhang EW. Dynamic monitoring of multi-year vegetation coverage in Sichuan province based on google earth engines. For Resour Manage. 2019;4:124–31. doi: 10.13466/j.cnki.lyzygl.2019.04.018.

[8] Taheri F, Jafari H, Rezaei M, Bagheri R. The use of continuous fuzzy and traditional classification models for groundwater potentiality mapping in areas underlain by granitic hard-rock aquifers. Environ Earth Sci. 2020;79(5):1–16. doi: 10.1007/s12665-020-8830-y.

[9] Jin XM, Liu JT, Wang ST, Xia W. Vegetation dynamics and their response to groundwater and climate variables in Qaidam Basin, China. Int J Remote Sens. 2016;37(3):710–28. doi: 10.1080/01431161.2015.1137648.

[10] Gao ZH, Li ZY, Wei HD, Ding F. Quantitative monitoring of vegetation cover change by using remotely sensed data over Minqin Oasis, Gansu. Geogr Res. 2006;25(4):587–93. doi: 10.3321/j.issn:1000-0585.2006.04.004.

[11] Yao Y, Wei X, Gao S, Jiang B, Zhao X. A review on fractional vegetation cover estimation using remote sensing. Adv Earth Sci. 2013;37(3):774–82. doi: 10.11867/j.issn.1001-8166.2013.07.0774.

[12] Zhang ZX, Deng RR, Li H, Chen L, Chen QD, He YQ. Remote sensing monitoring of vegetation coverage in southern China based on pixel unmixing: a case study of Guangzhou city. Remote Sens Land Resour. 2011;3:88–94. doi: CNKI:SUN:GTYG.0.2011-03-018.

[13] Zhou ZM, Yang YM, Chen BQ. Estimating Spartina alterniflora fractional vegetation cover and aboveground biomass in a coastal wetland using SPOT6 satellite and UAV data. Aquat Bot. 2018;144:38–45. doi: 10.1016/j.aquabot.2017.10.004.

[14] Li LL, Wang DW, Ham T. Spatial-temporal dynamics of vegetation coverage and responding to climate change in Shiyang River Basin during 2000–15. J Desert Res. 2018;38(5):212–22. doi: 10.7522/j.issn.1000-694X.2017.00061.

[15] Tao GF, Jia K, Zhao X, Wei XQ, Xie XH, Zhang XW, et al. Generating high spatio-temporal resolution fractional vegetation cover by fusing GF-1 WFV and MODIS data. Remote Sens. 2019;11(19):2324. doi: 10.3390/rs11192324.

[16] Qiao ZM, Wang XB, Yang L, Ma YG. Study on remote sensing inversion model of vegetation coverage using Landsat 8. J Qinghai Norm Univ (Nat Sci). 2019;35(1):59–63. doi: 10.16229/j.cnki.issn1001-7542.2019.01.009.

[17] Tucker CJ. Red and photographic infrared linear combinations for monitoring vegetation. Remote Sens Environ. 1979;8(2):127–50. doi: 10.1016/0034-4257(79)90013-0.
[18] Verrelst J, Schaepman ME, Koetz B, Kneubühler M. Angular sensitivity analysis of vegetation indices derived from CHRIS/PROBA data. Remote Sens Environ. 2008;112(5):2341–53. doi: 10.1016/j.rse.2007.11.001.
[19] Wang XQ, Wang MM, Wang SQ, Wu YD. Extraction of vegetation information from visible unmanned aerial vehicle images. Trans Chin Soc. Agric Eng. 2015;31(5):152–8. doi: 10.3969/j.issn.1002-6819.2015.05.022.
[20] Liu QY, Zhang TL, Li YZ, Li Y, Bu CF, Zhang QF. Comparative analysis of fractional vegetation cover estimation based on multi-sensor data in a semi-arid sandy area. Chin Geogr Sci. 2019;29(1):166–80. doi: 10.1007/s11769-018-1010-2.
[21] Niu BR, Liu JR, Wang ZW. Remote sensing information extraction based on vegetation fraction in drought and half-drought area. Geomatics Inf Sci Wuhan Univ. 2005;30(1):27–80. doi: 10.3321/j.issn:1671-8860.2005.01.007.
[22] Yue J, Mu GJ, Tang ZH, Yang XF, Lin YC, Xu LS. Remote sensing estimation models for vegetation coverage in desert regions of Xinjiang based on NDVI. Arid Land Geogr. 2020;43(1):153–60. doi: 10.12118/j.issn.1000-6060.2020.01.18.
[23] Kanke Y, Tubana B, Dalen M, Harrell D. Evaluation of red and red-edge reflectance-based vegetation indices for rice biomass and grain yield prediction models in paddy fields. Precis Agric. 2016;17(5):507–30. doi: 10.1007/s11119-016-9433-1.
[24] Li D, Cheng T, Zhou K, Zheng HB, Yao X, Tian YC, et al. WREP: a wavelet-based technique for extracting the red edge position from reflectance spectra for estimating leaf and canopy chlorophyll contents of cereal crops. ISPRS J Photogramm. 2017;129:103–17. doi: 10.1016/j.isprsjprs.2017.04.024.
[25] Forkuor G, Dimobe K, Serme I, Tondoh JE. Landsat-8 vs. Sentinel-2: examining the added value of sentinel-2's red-edge bands to land-use and land-cover mapping in Burkina Faso. Gisci Remote Sens. 2017;55(3):331–54. doi: 10.1080/15481603.2017.1370169.
[26] Thompson CN, Guo W, Sharma B, Ritchie GL. Using normalized difference red edge index to assess maturity in cotton. Crop Sci. 2019;59:2167–77. doi: 10.2135/cropsci2019.04.0227.
[27] Liu J, Wang LM, Teng F, Yang LB, Gao JM, Yao BM, et al. Impact of red-edge waveband of RapidEye satellite on estimation accuracy of crop planting area. Trans Chin Soc Agric Eng (Trans CSAE). 2016;32(13):140–8. doi: 10.11975/j.issn.1002-6819.2016.13.020.
[28] Li XJ, Chen G, Liu JY, Chen WT, Cheng XW, Liao YW. Effects of RapidEye imagery's red-edge band and vegetation indices on land cover classification in an arid region. Chin Geogr Sci. 2017;27:827–35. doi: 10.1007/s11769-017-0894-6.
[29] Kim HO, Yeom JM. Sensitivity of vegetation indices to spatial degradation of RapidEye imagery for paddy rice detection: a case study of South Korea. Gisci Remote Sens. 2015;5(1):1–17. doi: 0.1080/15481603.2014.1001666.
[30] She B, Huang J, Shi JJ, Wei CW. Extracting oilseed rape growing regions based on variation characteristics of red edge position. Trans Chin Soc Agric Eng (Trans CSAE). 2013;29(15):145–52. doi: 10.3969/j.issn.1002-6819.2013.15.018.
[31] Cai YT, Zhang M, Lin H. Estimating the urban fractional vegetation cover using an object-based mixture analysis method and sentinel-2 MSI imagery. IEEE J-Stars. 2020;13:341–50. doi: 10.1109/JSTARS.2019.2962550.
[32] Wang B, Jia K, Liang SL, Xie XH, Wei X, Zhao X, et al. Assessment of sentinel-2 MSI spectral band reflectances for estimating fractional vegetation cover. Remote Sens. 2018;10(12):1927. doi: 10.3390/rs10121927.
[33] Hua YC, Li ZY, Gao ZH. Variation of vegetation coverage in Minqin city since 2001. Arid Zone Res. 2017;34(2):337–43. doi: 10.13866/j.azr.2017.02.13.
[34] North PRJ. Estimation of f_{APAR}, LAI, and vegetation fractional cover from ATSR-2 imagery. Remote Sens Environ. 2002;80:114–21. doi: 10.1016/S0034-4257(01)00292-9.
[35] Xiao JF, Moody A. A comparison of methods for estimating fractional green vegetation cover within a desert-to-upland transition zone in central New Mexico, USA. Remote Sens Environ. 2005;98:237–50. doi: 10.1016/j.rse.2005.07.011.
[36] Yang Q, Wang TT, Chen H, Wang YD. Characteristics of vegetation cover change in Xilin Gol League based on MODIS EVI data. Trans Chin Soc Agric Eng (Trans CSAE). 2015;31(22):191–8. doi: 10.11975/j.issn.1002-6819.2015.22.026.
[37] Baloloy AB, Blanco AC, Ana RRCS, Nadaoka K. Development and application of a new mangrove vegetation index (MVI) for rapid and accurate mangrove mapping. ISPRS J Photogramm. 2020;166:95–117. doi: 10.1016/j.isprsjprs.2020.06.001.
[38] Jia K, Liang SL, Liu SH, Li YW, Xiao Z, Yao Y, et al. Global land surface fractional vegetation cover estimation using general regression neural networks from MODIS surface reflectance. IEEE Trans Geosci Remote. 2015;53(9):4787–96. doi: 10.1109/TGRS.2015.2409563.
[39] Hansen MC, DeFries RS, Townshend JRG, Carroll M, Dimiceli C, Sohlberg RA. Global percent tree cover at a spatial resolution of 500 meters: first results of the MODIS vegetation continuous fields algorithm. Earth Interact. 2003;7(1):1–15. doi: 10.3161/150811008X331063.
[40] Su LH. Optimizing support vector machine learning for semi-arid vegetation mapping by using clustering analysis. ISPRS J Photogramm. 2009;64:407–13. doi: 10.1016/j.isprsjprs.2009.02.002.
[41] Han D, Wang HZ, Zheng BY, Wang F. Vegetation type classification and fractional vegetation coverage estimation for an open elm (Ulmus pumila) woodland ecosystem during a growing season based on an unmanned aerial vehicle platform coupled with decision tree algorithms. Acta Ecol Sin. 2018;38(18):6655–63. doi: 10.5846/stxb201803300694.
[42] Liu DY, Yang LQ, Jia K, Liang SL, Xiao ZQ, Wei XQ, et al. Global fractional vegetation cover estimation algorithm for VIIRS reflectance data based on machine learning methods. Remote Sens. 2018;10:1648. doi: 10.3390/rs10101648.
[43] Guo YK, Liu YL, Zhang XJ, Xu M. LAI inversion using radiation transfer model and random forest regression. Eng Surv Map. 2019;28(6):17–21 + 29. doi: 10.19349/j.cnki.issn1006-7949.2019.06.004.
[44] Qi J, Marsett RC, Moran MS, Goodrich DC, Heilman P, Kerr YH, et al. Spatial and temporal dynamics of vegetation in the San Pedro River basin area. Agr For Meteorol. 2000;105:55–68. doi: 10.1016/S0168-1923(00)00195-7.
[45] Li MM, Wu BF, Yan CZ, Zhou WF. Estimation of vegetation fraction in the upper basin of Miyun reservoir by remote sensing. Resour Sci. 2004;26:153–9. doi: 10.1007/BF02973453.

[46] Cheng DY, Li XD. Vegetation coverage change in a karst area and effects of terrain and population. J Geo-Inf Sci. 2019;21(8):1227–39. doi: 10.12082/dqxxkx.2019.180548.
[47] Zhao GC, Li Z, Han ZX. Study on dynamic change of vegetation coverage in Beipiao city based on pixel bipartite model. Geomatics Spat Inf Technol. 2019;42(7):5–7. doi: 10.3969/j.issn.1672-5867.2019.07.002.
[48] Zhang XF, Liao CH, Li J, Sun Q. Fractional vegetation cover estimation in arid and semi-arid environments using HJ-1 satellite hyperspectral data. Int J Appl Earth Obs. 2013;21:506–12. doi: 10.1016/j.jag.2012.07.003.
[49] Wang J, Yan QW, Tan XL, Zou YQ. Vegetation coverage dynamics and its driving factors in inner Mongolia based on FVC information entropy. For Resour Manage. 2019;4:159–67. doi: 10.3466/j.nki.yzygl.019.4.23.
[50] Gao LM, Zhang LL. Spatiotemporal dynamics of the vegetation coverage in Qinghai Lake basin. J Geo-Inf Sci. 2019;21(9):1318–29. doi: 10.12082/dqxxkx.2019.180696.
[51] Pang GW, Yang QK, Wang CM, Shan LX, Wang BL. Influence of parameter determination methods of the pixel dichotomy model on the estimation accuracy of fractional vegetation cover by GF-1 PMS data. Geogr Geo-Inf Sci. 2019;35(4):27–33. doi: 10.3969/j.issn.1672-0504.2019.04.005.
[52] Shen Q, Zhu C, Zhang X. Fractional vegetation cover estimation in aird and rare vegetation area aided by GF-2 remote sensing data. Bull Surv Map. 2019;7:33–8. doi: 10.13474/j.cnki.11-2246.2019.0214.
[53] Meng CC, Zhao J, Lan YB, Lu LQ, Yang HB, Li ZM, et al. Vegetation coverage extraction model of winter wheat based on pixel dichotomy. J South China Agric Univ. 2020;41(3):126–32. doi: 10.7671/j.issn.1001-411X.201909005.
[54] Lu H, Xie YW, Zhang WP, Wei JJ. Spatiotemporal change of the oasis in Minqin county during the period from 1986 to 2015. Arid Zone Res. 2017;34(6):1410–7. doi: 10.13866/j.azr.2017.06.25.